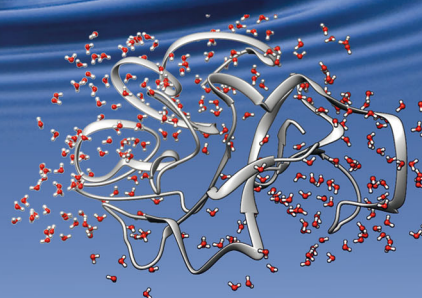
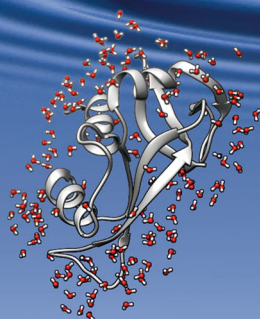
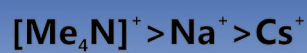
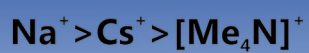


# PCCP

Physical Chemistry Chemical Physics

[www.rsc.org/pccp](http://www.rsc.org/pccp)



ISSN 1463-9076



## PAPER

Christian Herrmann, Simon Ebbinghaus *et al.*  
The temperature dependence of the Hofmeister series: thermodynamic fingerprints of cosolute–protein interactions

**175** YEARS



Cite this: *Phys. Chem. Chem. Phys.*,  
2016, **18**, 29698

# The temperature dependence of the Hofmeister series: thermodynamic fingerprints of cosolute–protein interactions†

Michael Senske,<sup>a</sup> Diana Constantinescu-Aruxandei,<sup>‡,b</sup> Martina Havenith,<sup>a</sup>  
Christian Herrmann,<sup>\*b</sup> Hermann Weingärtner<sup>a</sup> and Simon Ebbinghaus<sup>\*a</sup>

The Hofmeister series is a universal homologous series to rank ion-specific effects on biomolecular properties such as protein stability or aggregation propensity. Although this ranking is widely used, outliers and exceptions are discussed controversially and a molecular level understanding is still lacking. Studying the thermal unfolding equilibrium of RNase A, we here show that this ambiguity arises from the oversimplified approach to determine the ion rankings. Instead of measuring salt effects on a single point of the protein folding stability curve (e.g. the melting point  $T_m$ ), we here consider the salt induced shifts of the entire protein ‘stability curve’ (the temperature dependence of the unfolding free energy change,  $\Delta G_u(T)$ ). We found multiple intersections of these curves, pinpointing a widely ignored fact: the Hofmeister cation and anion rankings are temperature dependent. We further developed a novel classification scheme of cosolute effects based on their thermodynamic fingerprints, reaching beyond salt effects to non-electrolytes.

Received 21st July 2016,  
Accepted 22nd August 2016

DOI: 10.1039/c6cp05080h

www.rsc.org/pccp

## Introduction

The native conformation of a protein is only marginally stable.<sup>1</sup> The low stability is expressed by the low Gibbs free energy of unfolding,  $\Delta G_u = \Delta H_u - T\Delta S_u$ , which can be dissected into its enthalpic and entropic contributions,  $\Delta H_u$ , and  $T\Delta S_u$ , respectively.  $\Delta G_u$  forms the thermodynamic driving force of the transition from the native to the unfolded state and has to be positive for a stable conformation. The low  $\Delta G_u$  is founded in the mutual compensation of large enthalpic and entropic contributions, known as “enthalpy–entropy compensation”,<sup>2</sup> which can be manipulated by adding cosolutes.

The characterization of these cosolute effects is crucial to understand the role of species in the inner of the cell, which is densely crowded with (bio)-macromolecules up to 300 mg mL<sup>−1</sup>.<sup>3</sup> In general, cosolutes which are preferentially excluded from the protein surface favor the folded state because of its smaller solvent exposed surface. Cosolutes which preferentially bind to protein surfaces shift the equilibrium to the unfolded state.

Macromolecular crowders, such as polyethylene glycol or dextran, are thought to be excluded cosolutes. Proposed mechanisms range from entropic excluded volume effects<sup>4,5</sup> to enthalpic effects similar to osmolytes.<sup>6,7</sup> Osmolytes including polyols, sugars and amines stabilize proteins and protect the cellular proteome from environmental stresses.<sup>8</sup> They are excluded from protein surfaces and act mainly *via* an enthalpic stabilization mechanism.<sup>5,7,9</sup> On the other hand, chemical denaturants, such as guanidinium salts and urea, destabilize proteins by direct interactions which reduce  $\Delta H_u$ .<sup>7,10–12</sup>

Since Hofmeister’s observation<sup>13</sup> that salts precipitate hen egg-white proteins in a highly ion-specific manner, salt effects on proteins have received particular attention.<sup>14–18</sup> The resulting anion and cation rankings, known as “Hofmeister series”, are encountered in many fields of chemistry and biochemistry such as surface tension and potential,<sup>19,20</sup> orientational ordering of thermotropic liquid crystals at aqueous interfaces,<sup>21</sup> protein crystallization,<sup>22</sup> protein aggregation,<sup>23</sup> and enzymatic activity.<sup>24,25</sup> Anion and cation rankings for the effect of salts on protein stability are typically based on the propensity to stabilize/destabilize native proteins, using the “melting temperature”,  $T_m$ , of the protein as a criterion.<sup>14,26,27</sup>  $T_m$  is defined as the midpoint of the unfolding transition, where  $\Delta G_u = 0$ . There are, however, striking exceptions from Hofmeister behavior, such as an inverse anion series observed for hen egg-white lysozyme at low pH<sup>22,23,28</sup> and some ions that are difficult to integrate into the Hofmeister scheme.<sup>14,15</sup> Moreover, the ion-specificity

<sup>a</sup> Department of Physical Chemistry II, Ruhr-Universität Bochum, 44780 Bochum, Germany. E-mail: Simon.Ebbinghaus@rub.de

<sup>b</sup> Department of Physical Chemistry I, Ruhr-Universität Bochum, 44780 Bochum, Germany. E-mail: Chr.Herrmann@rub.de

† Electronic supplementary information (ESI) available. See DOI: 10.1039/c6cp05080h

‡ National Institute for R&D in Chemistry and Petrochemistry, Spl. Independentei 202, 060021 Bucharest, Romania.



is concentration dependent: while electrostatic effects are expected to be most significant at low concentrations,<sup>27,29,30</sup> ion-specific effects were observed both at low and high concentrations.<sup>31,32</sup>

Instead of focusing on the single state, where  $\Delta G_u = 0$ , the understanding of ion-specific effects is largely increased by determining  $\Delta G_u$  over a wide range of temperatures, obtaining the so-called “stability curve”  $\Delta G_u(T)$  of the protein. Standard thermodynamic procedures allow to dissect  $\Delta G_u(T)$  into its enthalpic and entropic parts,  $\Delta H_u(T)$  and  $T\Delta S_u(T)$ .<sup>33</sup> Cosolute-induced changes relative to the cosolute-free, buffered solution are then quantified by the excess functions:

$$\Delta\Delta G_u = \Delta G_{u,\text{cosolute}} - \Delta G_{u,\text{buffer}} = \Delta\Delta H_u - T\Delta\Delta S_u \quad (1)$$

We use here differential scanning calorimetry (DSC) to determine the excess free energy  $\Delta\Delta G_u$  and its contributions  $\Delta\Delta H_u$  and  $T\Delta\Delta S_u$ , which provide intriguing thermodynamic fingerprints of the different mechanisms of cosolute action. Such information is also crucial for developing and validating molecular level theories of ion-specific behavior.  $\Delta\Delta G_u$  is less suited for this purpose because different values of  $\Delta\Delta H_u(T)$  and  $T\Delta\Delta S_u(T)$  can result in the same value of  $\Delta\Delta G_u$ .

Specifically, we explore here effects of salts and of some nonelectrolytes on the unfolding thermodynamics of ribonuclease A (RNase A, 124 residues, 13.7 kDa). The ionic cosolutes range from simple alkali halides to complex low-melting organic salts (“ionic liquids”), which enable the systematic variation of the cosolute properties of the ions<sup>34</sup> and possess a high potential for steering biomolecular processes.<sup>35,36</sup> We have recently explored the impact of ionic liquids on unfolding of RNase A,<sup>37,38</sup> and their propensity to steer protein aggregation.<sup>39</sup> Since many questions applying to salt effects also concern neutral cosolutes, one gets insight into these mechanism by comparative studies, here especially for alcohols and osmolytic polyols.

## Materials and methods

Bovine pancreatic RNase A (type III-A) and the various cosolutes were obtained from different companies (see Table S1, ESI†). Stock solutions of RNase A in 50 mM citrate buffer at pH 5.0 were mixed with solutions containing the cosolute to obtain a protein concentration of 0.5 mg mL<sup>-1</sup>, which was controlled by UV-VIS spectroscopy at 280 nm, using a NanoDrop 2000 c spectrometer (Thermo Scientific, Waltham, USA). The unfolding transition was characterized by recording DSC thermograms at a rate of 90 K h<sup>-1</sup> by a VP-DSC instrument (MicroCal, Northampton, USA) and a Capillary-DSC apparatus (Malvern, Herrenberg, Germany). Our analysis also includes DSC thermograms of RNase A (5.0 mg mL<sup>-1</sup>) in 10 mM phosphate buffer at pH 5.5 in the presence of ionic liquids,<sup>37</sup> which were recorded at a scan rate of 60 K h<sup>-1</sup> (Table S1, ESI†). Complex cations used include tetramethylammonium ([Me<sub>4</sub>N]<sup>+</sup>), tetrabutylammonium ([Bu<sub>4</sub>N]<sup>+</sup>), 1-ethyl-3-methylimidazolium ([emim]<sup>+</sup>), 1-butyl-3-methylimidazolium ([bmim]<sup>+</sup>), 1-hexyl-3-methylimidazolium ([hmim]<sup>+</sup>), *N*-butylmethylpyrrolidinium ([bmpyr]<sup>+</sup>), choline ([chol]<sup>+</sup>).

Anions include dicyanamide ([dca]<sup>-</sup>), ethylsulfate ([EtSO<sub>4</sub>]<sup>-</sup>), dihydrogen phosphate ([dhp]<sup>-</sup>).

At pH ~ 5.0 RNase A (pI = 9.6) forms monomers with a charge of about +7,<sup>39</sup> which undergo a reversible two-state process, characterized by the equilibrium constant

$$K = e^{-\Delta G_u^0/RT} \quad (2)$$

where  $R$  is the gas constant and  $\Delta G_u^0$  the Gibbs free energy of unfolding in the standard state (index “0”). For simplicity this index “0” will be dropped throughout this paper. In DSC scans deviations from standard conditions are expected to be small.

The experimental observable is the partial heat capacity  $C_{p,\text{pr}}^{\text{exp}}$  of the protein obtained from the DSC thermogram after correction for the solvent contribution (see ESI,† S.1). Fits to the two-state model yielded  $T_m$ ,  $\Delta H_u(T_m)$ ,  $\Delta S_u(T_m) = \Delta H_u(T_m)/T_m$ , and the heat capacity change at  $T_m$ ,  $\Delta C_p(T_m)$ . For most measurements (Table S1, ESI†) the caloric enthalpy  $\Delta H_{u,\text{cal}}$  agreed with the van't Hoff enthalpy  $\Delta H_{u,\text{vH}}$  calculated from the temperature dependence of  $\Delta G_u$  to within 5% or better, as required for a two-state model.<sup>33</sup> Three repeated measurements in buffer were used to estimate the systematic error of all scans (Table S1, ESI†).

The temperature dependence of  $\Delta G_u$ ,  $\Delta H_u$  and  $\Delta S_u$  is given by Kirchhoff's laws (eqn (3)–(5)). In agreement with previous findings<sup>7</sup> the cosolutes did not significantly influence  $\Delta C_p(T_m)$  (see Table S2 and ESI,† S.2), which allows to approximate  $\Delta C_p(T)$  by the result obtained for the buffer solution.<sup>40</sup> Excess functions  $\Delta\Delta G_u$ ,  $\Delta\Delta H_u$  and  $T\Delta\Delta S_u$  ( $\Delta\Delta X = X_{\text{cosolute}} - X_{\text{buffer}}$ ) relative to buffer scans at equal condition were then calculated at  $T_{m,\text{buffer}}$  using eqn (3)–(5) and the temperature dependence of  $\Delta C_p$  (see ESI,† S.1). Different choices of buffer and variation of the pH in the range from 5 to 5.5 had only a small effect on  $T_m$  and  $\Delta H_u$  which canceled in the excess functions  $\Delta\Delta G_u$ ,  $\Delta\Delta H_u$  and  $T\Delta\Delta S_u$  and in  $\Delta T_m$ .

$$\Delta H^0(T) = \Delta H^0(T_m) + \int_{T_m}^T \Delta C_p^0 dT \quad (3)$$

$$\Delta S^0(T) = \Delta S^0(T_m) + \int_{T_m}^T \frac{\Delta C_p^0}{T} dT \quad (4)$$

$$\Delta G_u(T) = \Delta H_u(T_m) \left(1 - \frac{T}{T_m}\right) + \int_{T_m}^T \Delta C_p dT - T \int_{T_m}^T \frac{\Delta C_p}{T} dT \quad (5)$$

## Results

### Salt-induced changes of $T_m$

In Fig. 1 we illustrate the primary experimental data by baseline-corrected heat capacity scans of RNase A in 50 mM citrate buffer in the presence of stabilizing K[dhp] and destabilizing Na[ClO<sub>4</sub>], respectively. Based on such data, Fig. 2 gives an overview on salt effects on  $T_m$  of RNase A by plotting the cosolute-induced shift  $\Delta T_m = T_{m,\text{cosolute}} - T_{m,\text{buffer}}$  of the melting temperature *versus* the salt concentration. Charged proteins undergo electrostatic interactions with ions at very low concentrations, which result in protein destabilization at 0.25 and 0.5 M by almost all salts.



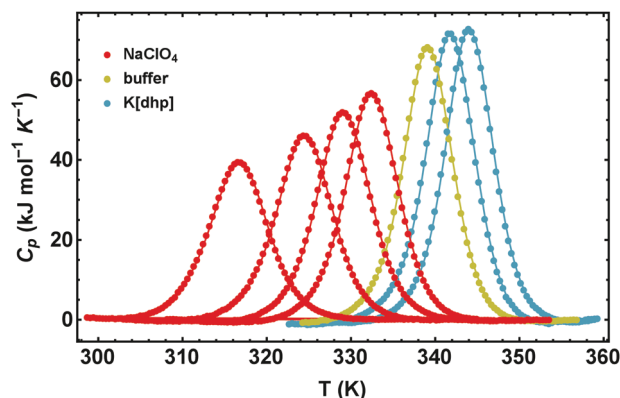


Fig. 1 Effect of  $\text{NaClO}_4$  and  $\text{K[dhp]}$  on the excess heat capacities of RNase A in 50 mM citrate buffer at pH 5.0. The data points are joined to guide the eye. From the left to the right the salt concentrations are 2 M, 1 M, 0.5 M, 0.25 M ( $\text{NaClO}_4$ ) and 0.25 M, 0.5 M ( $\text{K[dhp]}$ ).

However, our data for  $\text{K[dhp]}$  and  $[\text{chol}][\text{dhp}]$  (increase of  $\Delta T_m$  in the entire measured concentration range, Fig. 2f) indicate that ion-specific effects can also be dominant at these concentrations. At high salt concentrations ( $\geq 1$  M) electrostatic forces are screened and ion-specific effects become dominant. In the case of stabilizing salts one therefore expects a minimum of the concentration dependence of  $T_m$ , while destabilizing salts act in the same direction as the electrostatic effects and depress  $T_m$ .

Shallow minima of  $T_m$  near 0.5 M (e.g.  $\Delta T_m \cong -2$  K for 0.5 M  $\text{NaCl}$ ) were indeed observed for stabilizing alkali metal chlorides,  $[\text{Me}_4\text{N}]\text{Cl}$  and  $[\text{chol}]\text{Cl}$  (Fig. 2a). For salts with

oxo-anions, such as  $\text{K}_2[\text{SO}_4]$ ,  $\text{K[dhp]}$  and  $[\text{chol}][\text{dhp}]$  (Fig. 2f), the stabilizing ion-specific effects are too strong to trace these minima. For  $\text{LiCl}$  (Fig. 2b) and  $\text{NaBr}$  (Fig. 2d)  $T_m$  decreases, but an inflection point of the concentration dependence is still reminiscent of the minima in Fig. 2a. For stronger destabilizing agents, such as  $\text{Na}[\text{ClO}_4]$ ,  $T_m$  decreases monotonously. Most ionic liquids destabilize proteins as well. As the alkyl chains of the cation increase in length, the destabilizing power of ionic liquids increases rapidly and leads to a largely negative  $\Delta T_m$  (Fig. 2c). However, strong destabilization can also be enforced by anions, such as  $[\text{dca}]^-$  and  $[\text{SCN}]^-$  (Fig. 2e).

### Cosolute-induced changes of $\Delta G_u$

The proper thermodynamic driving force of the unfolding transition is the excess free energy  $\Delta\Delta G_u$ . Fig. 3 shows  $\Delta\Delta G_u$  for some alkali metal salts and ionic liquids at the temperature  $T_{m,\text{buffer}}$  as a function of salt concentration. In dilute solutions ( $< 0.25$  M) electrostatic interactions result in  $\Delta\Delta G_u < 0$ , while at higher salt concentrations stabilizing ion-specific effects ( $\Delta\Delta G_u > 0$ ) or destabilizing effects ( $\Delta\Delta G_u < 0$ ) become dominant, in parallel to the behavior of  $\Delta T_m$  displayed in Fig. 2. Considering this parallelism in more detail, we find an apparent linear relationship between  $\Delta\Delta G_u$  and  $\Delta T_m$  (even though it is a nonlinear relation). For details we refer to Fig. S1 (ESI†).

### Cosolute-induced changes of $\Delta H_u$ and $\Delta S_u$

Fig. 4 illustrates the dissection of  $\Delta\Delta G_u$  into its enthalpic and entropic parts,  $\Delta\Delta H_u$  and  $T\Delta\Delta S_u$ , by showing representative results for the various salt families. The excess functions  $\Delta\Delta H_u$

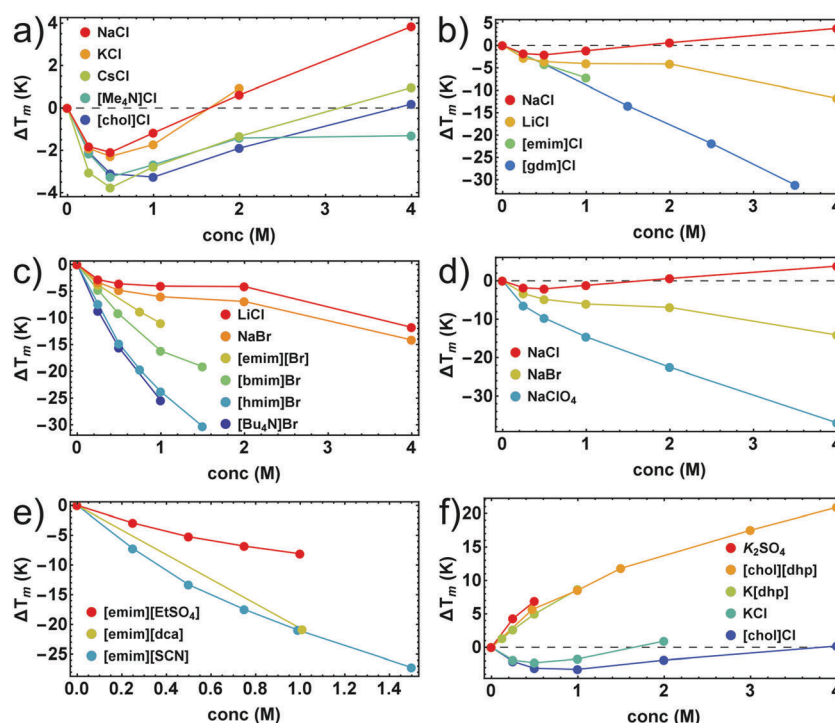


Fig. 2 Salt-induced shifts of  $T_m$  of RNase A. (a and b) chlorides; (c) bromides; (d) sodium salts; (e) salts with  $[\text{emim}]^+$  as cation; (f) salts with stabilizing oxo-anions. Error bars were calculated by Gaussian error propagation of the primary error estimates (see ESI†, S.1) and are smaller than the point size. Data points for  $\text{K}_2\text{SO}_4$  and  $[\text{gdm}]\text{Cl}$  were taken from Ravindra and Winter.<sup>41</sup>



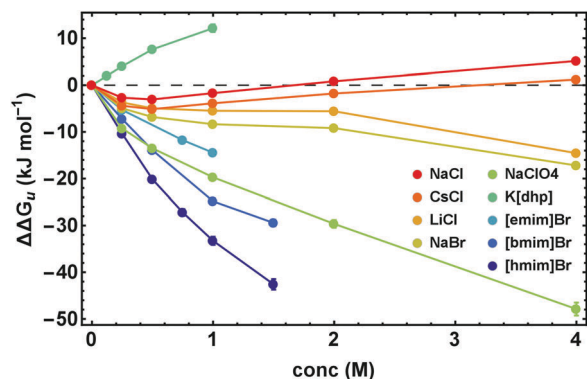


Fig. 3  $\Delta\Delta G_u$  calculated at  $T_m$  in cosolute-free solution,  $T_{m,buffer}$ , as a function of salt concentration. Error bars were calculated by Gaussian error propagation of the primary error estimates (see ESI,† S.1).

and  $T\Delta\Delta S_u$  behave highly salt-specific. For NaCl  $\Delta\Delta H_u$  and  $T\Delta\Delta S_u$  decrease monotonously with increasing salt concentration and are strongly coupled. In the case of [chol][dhp] both,  $\Delta\Delta H_u$  and  $T\Delta\Delta S_u$  initially increase and pass maxima. Their behavior parallels one another, but  $\Delta\Delta H_u$  becomes considerably larger than  $T\Delta\Delta S_u$ , leading to high values of  $\Delta\Delta G_u$ . For destabilizing Na[ClO<sub>4</sub>] the behavior is inverse. The curves initially decrease and pass minima at a concentration near 1 M. Both,  $\Delta\Delta H_u$  and  $T\Delta\Delta S_u$ , retain the same shape, but  $T\Delta\Delta S_u$  increases more strongly than  $\Delta\Delta H_u$  and eventually becomes positive, rendering  $\Delta\Delta G_u$  strongly negative. Finally, for more hydrophobic salts, here exemplified by [bmim]Br, both  $\Delta\Delta H_u$  and  $T\Delta\Delta S_u$  increase with concentration, but  $T\Delta\Delta S_u$  strongly dominates over  $\Delta\Delta H_u$ .

Further insight into these issues is gained by an entropy–enthalpy compensation plot of  $T\Delta\Delta S_u$  versus  $\Delta\Delta H_u$  shown in Fig. 5. This diagram characterizes the mutual compensation of large enthalpic and entropic contributions, which tend to cancel in  $\Delta G_u$ . Different signs of the excess functions  $\Delta\Delta G_u$ ,  $\Delta\Delta H_u$  and  $T\Delta\Delta S_u$ , define eight different fields in this plot which

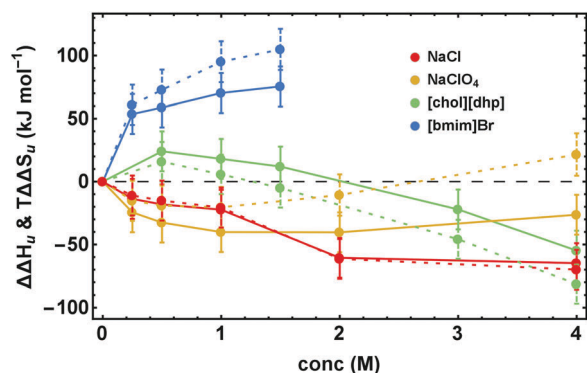


Fig. 4 Concentration dependence of  $\Delta\Delta H_u$  (data points connected by solid lines) and  $T\Delta\Delta S_u$  (data points connected by dashed lines). Error bars were calculated by Gaussian error propagation of the primary error estimates (see ESI,† S.1). Note,  $\Delta\Delta H_u$  and  $T\Delta\Delta S_u$  are coupled ( $\Delta S_u(T_m) = \Delta H_u(T_m)/(T_m)$ ). Therefore, the error of the relative position of  $\Delta\Delta H_u$  and  $T\Delta\Delta S_u$  with respect to each other is much smaller and is given by the errors of  $\Delta\Delta G_u$  in Fig. 3.

are marked by different colors. The blue diagonal corresponds to full enthalpy–entropy compensation and separates the protein destabilizing region ( $\Delta\Delta G_u < 0$ ) from the stabilizing region ( $\Delta\Delta G_u > 0$ ). Positive (negative) values of  $\Delta\Delta H_u$  imply stabilization (destabilization) by the cosolute. The entropy term acts in the opposite direction: a positive  $T\Delta\Delta S_u$  supports destabilization.

The sections I (magenta), and II (blue) and the sections V (yellow) and VI (orange) are most populated due to largely compensating enthalpic and entropic contributions. All hydrophobic ionic liquids (here the cations with butyl side chain or longer) fall into the magenta segment I, where  $\Delta\Delta H_u$  is positive, but  $T\Delta\Delta S_u$  is even more positive, leading to entropic destabilization offset by enthalpic stabilization. Hydrophilic salts (e.g. alkali halides) populate states near the borderline between sections V (yellow) and VI (orange), where both, the enthalpic as well as the entropic contribution are negative. Depending on the magnitudes of  $T\Delta\Delta S_u$  and  $\Delta\Delta H_u$ , one obtains stabilizing salts ( $\Delta\Delta G_u > 0$  in section V) or destabilizing salts ( $\Delta\Delta G_u < 0$  in section VI). The chemical denaturants [gdm]Cl and urea also fall in section VI. Some chlorides intersect the borderline from destabilizing to stabilizing behavior at high concentrations (see also Fig. 2 and 3).

As already observed in Fig. 2, strongly stabilizing salts based on oxo-anions, such as [dhp]<sup>−</sup>, reveal unique behavior. We have recently introduced [chol][dhp] as a highly soluble (biocompatible) substitute for K[dhp].<sup>35,39</sup> In Fig. 5 [chol][dhp] reveals a strongly non-monotonous behavior with a sharp transition from predominant enthalpic to entropic stabilization near 0.5 M (similar to K[dhp] at 0.25 M), which is associated with a maximum of  $\Delta\Delta H_u$  and  $T\Delta\Delta S_u$ . Two data points for K<sub>2</sub>SO<sub>4</sub> at 0.25 and 0.5 M reported by Ravindra and Winter<sup>41</sup> are also consistent with a very strong entropic stabilization. Na[ClO<sub>4</sub>] shows a non-monotonous behavior as well, but is strongly destabilizing and covers the segments VI and VII.

In principle,  $\Delta\Delta H_u$  and  $\Delta\Delta S_u$  (here calculated at  $T_{m,buffer}$ ) are temperature dependent, but the assumption  $\Delta C_{p,cosolute}(T) = \Delta C_{p,buffer}(T)$  used in our modellings renders  $\Delta\Delta H_u$  temperature independent and simplifies the expression for  $\Delta\Delta S_u$  to  $\Delta\Delta S_u = T\Delta C_p \ln(T_{s,buffer}/T_{s,cosolute})$ , where  $T_s$  is the temperature of maximum stability,  $\Delta G_{u,max}$ . Thus,  $\Delta\Delta H_u$  does not change with temperature and  $\Delta\Delta S_u$  does not change its sign.

### Temperature dependence of $\Delta G_u$

Because conformational stability requires  $\Delta G_u > 0$ , the temperature dependence of the stability curve  $\Delta G_u(T)$  represents a highly useful measure of the conformational stability. Fig. 6 pinpoints the basic features of  $\Delta G_u(T)$  and shows some typical examples for its response to added salts and neutral cosolutes. In general,  $\Delta G_u(T)$  resembles a parabola and intersects the zero line at high and low temperatures, defining  $T_m$  and the cold denaturation temperature  $T_c$ , respectively. For RNase A at pH 5–5.5 we extrapolate  $T_c$  to be < 200 K. Like for most other proteins,<sup>42</sup>  $T_c$  falls largely below the liquid range of the solution. Between  $T_c$  and  $T_m$  the stability curve passes a maximum, which gives access to  $T_s$  and  $\Delta G_{u,max}$ .



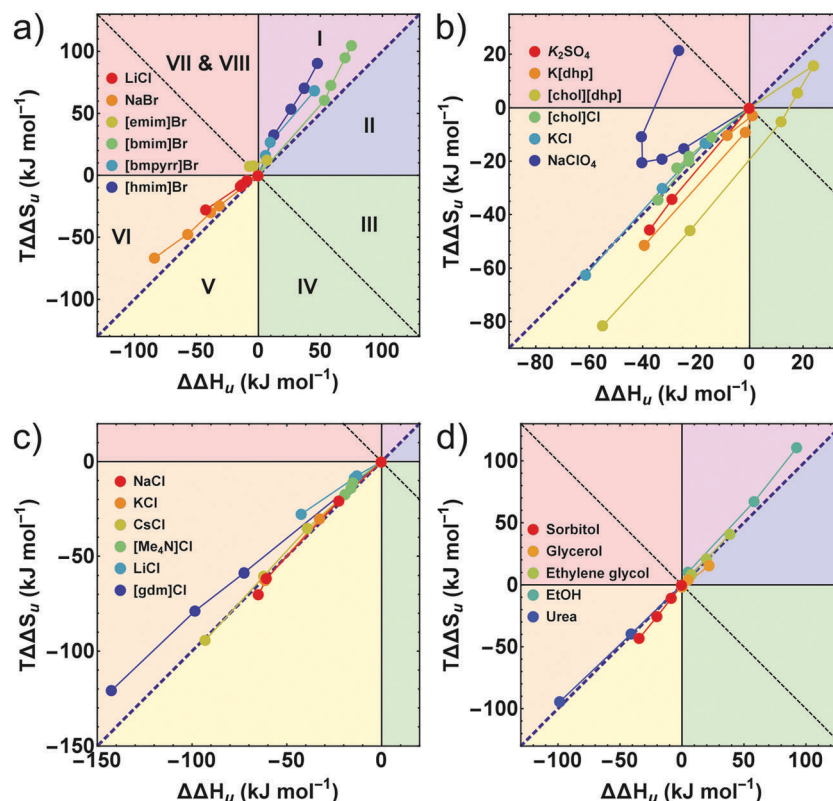


Fig. 5 (a–d) Enthalpy–entropy compensation plots. The different segments correspond to different contributions of  $\Delta\Delta G_u$ ,  $\Delta\Delta H_u$ , and  $T\Delta\Delta S_u$ . The blue diagonal corresponds to a complete enthalpy–entropy compensation. Data points correspond to different concentrations of the respective cosolute. (a, c and d) The first or the first two data points ( $\leq 0.5$  M) of some compounds are omitted for clarity. Error bars are coupled and omitted for clarity (see caption of Fig. 4). Data of [gdm]Cl, urea,  $K_2SO_4$ , and sorbitol are taken from Ravindra and Winter.<sup>41</sup>

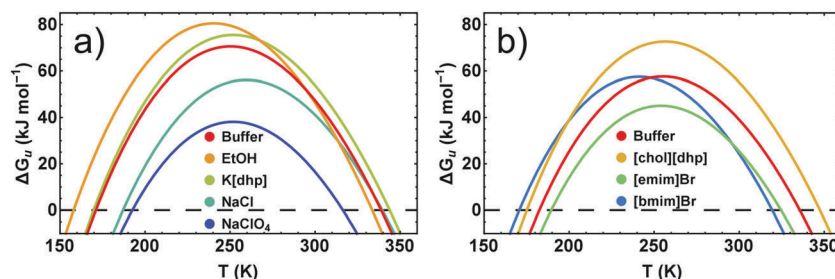


Fig. 6 Stability curves of RNase A in the presence of representative cosolutes. (a) RNase A in 50 mM citrate buffer at pH 5.0. (b) RNase A in 10 mM phosphate buffer at pH 5.5. The differences of the buffer curves are due to the higher concentration of the citrate buffer and a higher protein stabilizing propensity of the citrate compared to the phosphate ion.<sup>14</sup>

We have previously shown that the temperature dependence of  $\Delta C_p$  is crucial when calculating  $\Delta\Delta H_u$  and  $T\Delta\Delta S_u$  via eqn (3)–(5).<sup>7</sup> By contrast, the temperature dependence of  $\Delta G_u$  can be reliably estimated using a constant value for  $\Delta C_p$  (see Fig. S2, ESI<sup>†</sup>), which enables an estimate of  $\Delta G_u$  at temperatures at which measurement of  $\Delta C_p(T)$  are infeasible. Here we used  $\Delta C_p = 5.0 \text{ kJ K}^{-1} \text{ mol}^{-1}$ , resembling  $\Delta C_p$  of RNase A around room temperature.<sup>40</sup> If the cosolute does not alter  $\Delta C_p(T)$ ,  $\Delta\Delta G_u(T)$  deduced from the stability curve reflects the correct temperature dependence, and the shape of the stability curve is not affected by the cosolute ( $\partial^2 \Delta G_u(T)/\partial T^2 = -\Delta C_p(T)$ ). The discussion of cosolute-induced changes of  $\Delta G_u(T)$  can

therefore be reduced to the vertical and horizontal changes of the maximum protein stability,  $\Delta G_u(T_s)$  (Fig. 7 and 8).

### Maximum protein stability

In Fig. 7 and 8 we plot the vertical change of  $\Delta G_u(T_s)$ ,  $\Delta\Delta G_{u,\max}$ , versus the horizontal change,  $\Delta T_s$ , for all cosolutes. At the maximum of the stability curve  $\partial \Delta G_u(T)/\partial T$  is zero. Since  $\partial \Delta G_u(T)/\partial T = -\Delta S_u$  the maximum stabilization of a protein is purely enthalpic. Therefore, a vertical shift of the stability curve along the y-axis signals a purely enthalpic process ( $\Delta\Delta S_u = 0$ ), while a horizontal shift usually affects both, enthalpy and entropy.



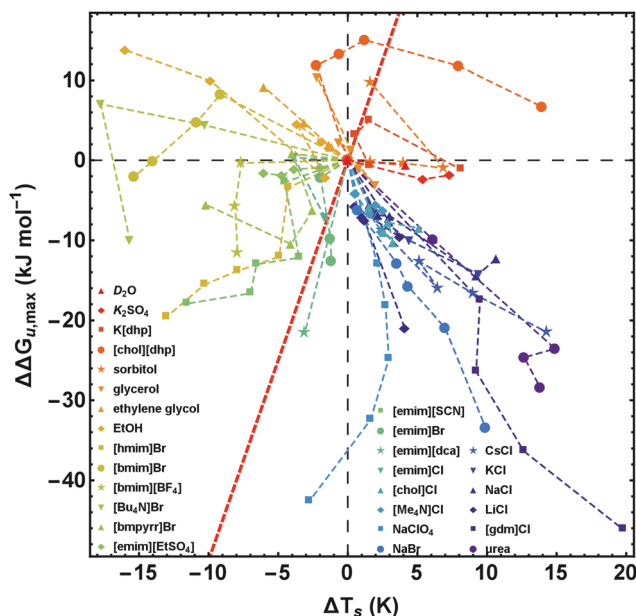


Fig. 7 Salt-induced changes of the maximum of the stability curve.  $\Delta\Delta G_{u,\max}$  corresponds to the vertical shift and  $\Delta T_s$  to the horizontal shift of the maximum position. To retain simplicity, salt concentrations are not given in the figure, but the sequence of concentrations is the same as in Fig. 2. While the red line ( $\Delta\Delta G_{u,\max}(\Delta T_s) = \Delta C_p \times \Delta T_s$ ) represents a pure entropic effect, the y-axis corresponds to a pure enthalpic effect. Error bars are omitted for clarity, but are given in Fig. 8 for a representative data point of each curve. Data of [gdm]Cl, urea,  $K_2SO_4$ , and sorbitol are taken from Ravindra and Winter.<sup>41</sup>

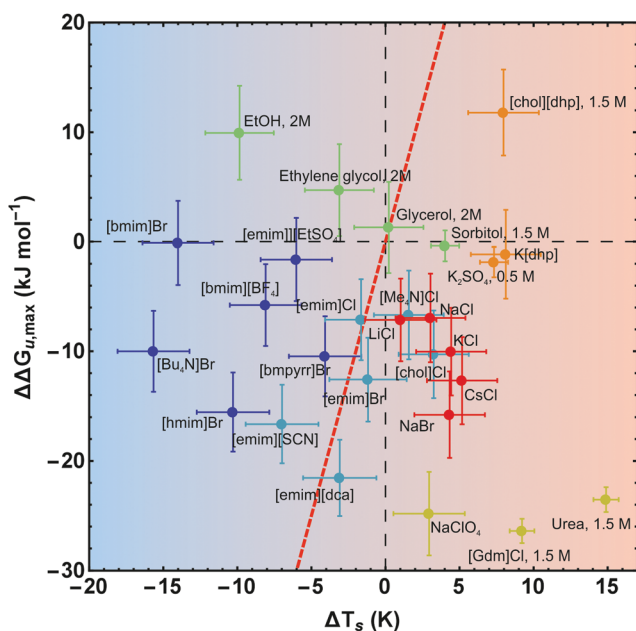


Fig. 8 Salt-induced changes of the maximum of the stability curve. If not stated otherwise, the concentration of the cosolutes is 1 M. The gradient of the background from blue to red color scales with increasing/decreasing hydrophilicity/hydrophobicity. While the red line ( $\Delta\Delta G_{u,\max}(\Delta T_s) = \Delta C_p \times \Delta T_s$ ) represents a pure entropic effect, the y-axis corresponds to a pure enthalpic effect. Error bars were calculated by Gaussian error propagation of the primary error estimates (see ESI† for details). Data of [gdm]Cl, urea,  $K_2SO_4$ , and sorbitol are taken from Ravindra and Winter.<sup>41</sup>

The red dashed line in Fig. 7 and 8 corresponds to the special case of a purely entropic effect (*i.e.*  $\Delta\Delta H_u = 0$ ).

There is a bundle of curves for alkali metal halides, which reduce  $\Delta G_{u,\max}$ , but increase  $T_s$ , thus falling into the lower right quarter of Fig. 7, where the cosolute mechanisms are characterized by enthalpic destabilization and entropic stabilization. In this regime, we also find the widely used denaturants urea and [gdm]Cl. While urea and [gdm]Cl are on the right hand side of the curves in the lower right quarter, the strong denaturant  $Na[ClO_4]$  is found on the left hand side close to purely enthalpic behavior. Another bundle of curves is associated with hydrophobic behavior of ionic liquids, which fall into the lower to the upper left quarter of Fig. 7. The two ionic liquids [bmim]Br and  $[Bu_4N]Br$  cross the abscissa corresponding to stability curves, where the maximum free energy is larger than that of the buffer solution. The latter regime is also populated by the neutral cosolutes ethanol and ethylene glycol, which are more hydrophobic than the larger polyols considered.

Summarizing these results, Fig. 8 compares the impact of all cosolutes considered in our study on  $\Delta G_{u,\max}$  at typical concentrations of 1–2 M. The major difference between hydrophilic salts (red symbols) and hydrophobic salts (blue symbols) is founded in a transition from entropic stabilization ( $\Delta T_s > 0$ ) to entropic destabilization ( $\Delta T_s < 0$ ). The same is true for the neutral cosolutes, where glycerol marks the borderline between entropic stabilization and destabilization. Although we are not aware of cosolutes that exhibit a purely enthalpic or purely entropic mechanism, there is a band of salts of low hydrophobicity which are close to these limits (light blue symbols and  $Na[ClO_4]$ ). In the latter cases destabilization seems substantially affected by the anion (*e.g.*  $[SCN]^-$ ,  $[dca]^-$ ,  $[ClO_4]^-$ ).

## Discussion

### Thermodynamic fingerprints

In general, the cosolute effect of salts on protein stability depends on the charge of the protein and is determined mainly by two effects. Electrostatic (coulombic) effects dominate at low concentrations and ion-specific (Hofmeister) effects at high concentrations.<sup>27,29,30</sup> Since the cosolutes effect of inorganic salts is largely influenced by specific salt–protein interactions the thermodynamic fingerprints of proteins in the presence of inorganic salts can be different. For positively charged RNase A in the presence of alkali halides we find enthalpic destabilization and entropic stabilization. The positively charged peptide met16 shows the same behavior of  $\Delta\Delta G_u$ , but thermodynamics reveals a different mechanism: the peptide is stabilized enthalpically, but destabilized entropically.<sup>30</sup> Yet another type of behavior is exhibited by positively charged ubiquitin. In the latter case the protein is stabilized *via* an enthalpic mechanism even at low concentrations of alkali and alkaline earth halides, at which electrostatic effects should prevail.<sup>7,43</sup>

While for positively charged RNase A in this study, anionic effects prevail over cationic effects, for negatively charged



RNase T1 the salt effect seems to result mainly from the interaction with the cations.<sup>44</sup> However, anions can strongly affect negatively charged proteins, specifically in the case of an extended positively charged amino acid cluster<sup>31</sup> or the existence of specific anion binding sites.<sup>45</sup> For in sum uncharged proteins, the overall salt effect seems to be weakened.<sup>7</sup>

For simple inorganic salts the variation of the cation has only a small effect on the stability of positively charged RNase A. On the other hand, cation variation of ionic liquids can lead to very strong effects (Fig. 2) because the thermodynamic mechanism depends on the hydrophobicity of the cation (Fig. 5a, 7 and 8). The longer the hydrophobic side chain of the cation, the stronger the destabilization at the high temperature end of the stability curve. These findings are not limited to RNase A. Actually, it seems that ionic liquids, at least the so-called aprotic ones,<sup>34</sup> destabilize proteins at the high temperature end of the stability curve.<sup>46–48</sup> The recently reported stabilization of  $\alpha$ -chymotrypsin by benzyl-methyl-imidazolium chloride<sup>49</sup> does not contradict this observation: although the overall effect on  $\Delta\Delta G_u$  is stabilizing,  $\alpha$ -chymotrypsin shows the typical thermodynamic fingerprint exhibited by RNase A and BSA<sup>47</sup> in the presence of ionic liquids: the enthalpic contribution is stabilizing, the entropic contribution is destabilizing.

It is interesting to compare these findings with data for some OH-bonded neutral cosolutes. Osmolytes like sorbitol or glycerol are known to increase  $T_m$ . According to the current opinion they stabilize proteins *via* an enthalpic mechanism.<sup>5,7</sup> For RNase A several studies report, however, a stabilization *via* an entropic pathway.<sup>50–52</sup> Our data for salts help to rationalize this discrepancy by comparing the enthalpy–entropy compensation of homologous alcohols and three polyols which differ in the number of OH-groups. We find that the nonelectrolytes reveal the same correlation between the hydrophobicity of the cosolute and the cosolute effects as observed for ionic liquids: the more hydrophobic the cosolute (*e.g.* ethanol) the stronger the reduction of  $T_m$  (Fig. S3, ESI†). The same trend holds for the enthalpy and entropy contributions: the more hydrophobic the cosolute, the larger the destabilizing entropic and the stabilizing enthalpic contribution (Fig. 5d). While ethanol induces an

entropic destabilization which is counteracted by an enthalpic stabilization, sorbitol stabilizes RNase A entropically and the enthalpic contribution is even destabilizing. For alcohols as cosolutes a positive  $\Delta\Delta H_u$  and  $\Delta\Delta S_u$  seems to be a general phenomenon.<sup>53–56</sup>

Our analysis also implies that the cosolute effects of ethanol and typical excluded osmolytes are not as different as it might appear at a first glance from the reduction of  $T_m$ . Ethanol shifts the stability curve upwards (Fig. 6a), which is typical for excluded cosolutes.<sup>57,58</sup> As shown in Fig. 8, the hydrophobicity/hydrophilicity determines the horizontal position of the maximum ( $T_s$ ). The more hydrophobic the cosolute, the larger the shift of  $T_s$  to lower temperatures, resulting in the discussed enthalpy–entropy compensation. While for RNase A in 4 M ethanol  $\Delta T_s = -16$  K, the addition of 2.5 M sorbitol shifts  $T_s$  even to higher temperatures compared to the buffer solution ( $\Delta T_s = 6.9$  K). Martin *et al.* have reported similar effects for yeast frataxin in alcohol solutions.<sup>55</sup>

In summary, combining the results for alkali halides, ionic liquids and alcohols/polyols, the stability curve of RNase A can be shifted in all possible directions scaling with the hydrophobicity of the cosolute (Fig. 7 and 8), which results in different thermodynamic fingerprints for these important classes of cosolutes. Thereby, the thermodynamic fingerprint of proteins in inorganic salt solution is a fingerprint of both, the protein and the salt, while the scaling of protein thermodynamics with hydrophobicity of the cosolutes is almost protein independent. Regarding protein stability, ionic liquids can be classified as a class of cosolutes in between inorganic salts and nonelectrolytes.

### Generalized Hofmeister series

An intriguing question is, how our results affect the current picture of ion-specific (Hofmeister) effects. For this purpose we adopt the cation and anion series of Collins and Washabaugh<sup>14</sup> as a reference, which are mainly based on data for salt effects on  $\Delta T_m$  by von Hippel and Schleich.<sup>26</sup> This criterion reflects the correct thermodynamic driving force since, as shown above,  $\Delta T_m$  is correlated with  $\Delta\Delta G_u$  (Fig. S1, ESI†). If  $\Delta\Delta G_u$  is dissected into its enthalpic and entropic contributions,  $\Delta\Delta H_u$ , and  $T\Delta\Delta S_u$ , the appealing simplicity and universality of the Hofmeister series immediately gets lost indicating heterologous molecular mechanisms.

We now compare the ion rankings deduced from  $\Delta T_m$ ,  $\Delta\Delta G_u$ ,  $\Delta\Delta H_u$ , and  $T\Delta\Delta S_u$ , respectively. Moreover, we expand this comparison to some complex ions, which are frequently used in the field of ionic liquids. As for most salts/ionic liquids the concentration dependence of  $\Delta\Delta G_u$ ,  $\Delta\Delta H_u$ , and  $T\Delta\Delta S_u$  is highly non-linear and often non-monotonous, we compare these properties at a given concentration of 1 M, which is high enough to ignore electrostatic contributions,<sup>30</sup> but not yet affected by the limited solubilities exhibited by some salts and ionic liquids. Ranking the ions at the melting temperature of the salt-free protein from their stabilizing to destabilizing propensity, the formulation of Collins and Washabaugh<sup>14</sup> predicts for the salts considered here the “direct” cation series:  $[\text{Me}_4\text{N}]^+$ ,  $\text{Cs}^+$ ,  $\text{K}^+$ ,  $\text{Na}^+$ ,  $\text{Li}^+$ ,  $[\text{gdm}]^+$ . There is, however, mounting

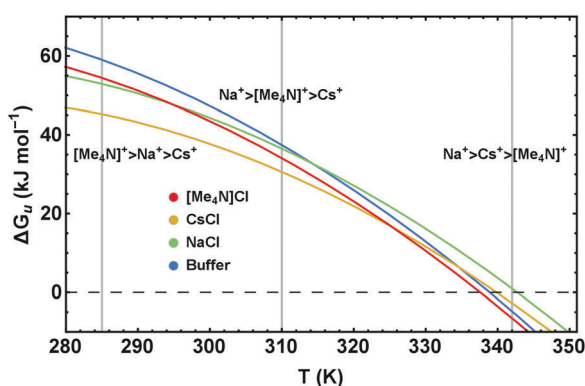


Fig. 9 Stability curves,  $\Delta G_u(T)$ , of RNase A in buffered solutions of 4 M NaCl, CsCl, and  $[\text{Me}_4\text{N}]\text{Cl}$  illustrating the temperature dependence of the Hofmeister series.





evidence that at  $\text{pH} < \text{pI}$ , this sequence is reversed.<sup>16,22,23,28,59</sup> This reversal is well established for anions, but work by Boström *et al.*<sup>28</sup> and Schwierz *et al.*<sup>59</sup> indicates a similar tendency for cations. In our study, where  $\text{pH} < \text{pI}$ , we find the following cation rankings at 1 M:

$\Delta T_m$ :	$\text{Na}^+, \text{K}^+, \text{Cs}^+ \approx [\text{Me}_4\text{N}]^+, \text{Li}^+, [\text{gdm}]^+$	(Inverse)
$\Delta\Delta G_u$ :	$\text{Na}^+, \text{K}^+, \text{Cs}^+ \approx [\text{Me}_4\text{N}]^+, \text{Li}^+, [\text{gdm}]^+$	(Inverse)
$\Delta\Delta H_u$ :	$\text{Li}^+ \approx [\text{Me}_4\text{N}]^+, \text{Na}^+, \text{K}^+, \text{Cs}^+, [\text{gdm}]^+$	(Inverse)
$T\Delta\Delta S_u$ :	$[\text{gdm}]^+, \text{Cs}^+, \text{K}^+, \text{Na}^+, [\text{Me}_4\text{N}]^+, \text{Li}^+$	(Direct)

Our results for  $\Delta T_m$  and  $\Delta\Delta G_u$  indeed reflect an inverse behavior, but  $\text{Li}^+$  and  $[\text{gdm}]^+$  are out of order. The motif  $\text{NaCl} > \text{KCl} > \text{LiCl} > [\text{gdm}]\text{Cl}$  exhibited by  $\Delta T_m$  and  $\Delta\Delta G_u$  has also been observed for a small model peptide by Sukenik *et al.*<sup>30</sup> The  $\Delta\Delta H_u$  data yield an inverse series with  $[\text{Me}_4\text{N}]^+$  and  $[\text{gdm}]^+$  out of order. By contrast, the results for  $T\Delta\Delta S_u$  resemble the direct series with  $[\text{Me}_4\text{N}]^+$  being out of order, thus essentially being opposite to those based on the  $\Delta\Delta H_u$  data.

It has been known before<sup>15</sup> that  $[\text{gdm}]^+$  is difficult to incorporate into the Hofmeister scheme, and in some Hofmeister studies reviewed by Collins and Washabaugh,<sup>14</sup> the positions of  $[\text{Me}_4\text{N}]^+$  and  $\text{Li}^+$  seem anomalous as well. Based on our dissection of  $\Delta\Delta G_u$  into  $\Delta\Delta H_u$  and  $T\Delta\Delta S_u$ , we can come up with an explanation for  $[\text{Me}_4\text{N}]^+$  being out of order: the hydrophobic character of the four methyl groups causes an up- and left-shift of the stability curve of RNase A compared to its expected position from the Hofmeister ranking. As already suggested by Flores *et al.*<sup>60</sup> and Schwierz *et al.*,<sup>61</sup> the anomalous behavior of  $\text{Li}^+$  can be rationalized by the tight binding of water molecules in the first hydration shell to the  $\text{Li}^+$ -ion which decreases the surface charge density. As a consequence, the ion appears to be more hydrophobic as suggested by the coincidence of the data points of  $\text{LiCl}$  and  $[\text{Me}_4\text{N}]\text{Cl}$  in Fig. 8.

Turning to effects exerted by some complex anions, which are frequently used in the field of ionic liquids, the observed rankings are

$\Delta T_m$ :	$[\text{EtSO}_4]^- , \text{Br}^- , [\text{dca}]^- \approx [\text{SCN}]^-$	(Direct)
$\Delta\Delta G_u$ :	$[\text{EtSO}_4]^- , \text{Br}^- , [\text{dca}]^- \approx [\text{SCN}]^-$	(Direct)
$\Delta\Delta H_u$ :	$[\text{EtSO}_4]^- , [\text{SCN}]^- , [\text{dca}]^- \approx \text{Br}^-$	(Inconclusive)
$T\Delta\Delta S_u$ :	$\text{Br}^- , [\text{dca}]^- , [\text{EtSO}_4]^- , [\text{SCN}]^-$	(Inconclusive)

Noting the extremely denaturing role of  $[\text{SCN}]^-$  based salts in the classical Hofmeister series,<sup>15</sup> a strong similarity of solution properties of salts containing  $[\text{dca}]^-$  and  $[\text{SCN}]^-$  and a fairly hydrophilic nature of  $[\text{EtSO}_4]^-$ ,<sup>34</sup> the results for  $\Delta T_m$  and  $\Delta\Delta G_u$  may conform to an extension of the direct series, while the results for  $T\Delta\Delta S_u$  and  $\Delta\Delta H_u$  are inconclusive and not in opposite direction. These observations are in line with previous bio-electrochemistry studies by Medda *et al.*, who found that the apparent Hofmeister ranking gets lost upon dissection of the redox potential of cytochrome *c* into the enthalpic and entropic contributions.<sup>62</sup>

## Temperature dependence of Hofmeister effects

Our results clearly show that for a proper understanding of Hofmeister behavior it is crucial to account for the temperature dependence of the cosolute effects. Translation of the different excess functions into stability curves (Fig. 6 and 9) reveals an important result which, according to our knowledge, has so far not been addressed in detail: the Hofmeister series is temperature dependent.

Using as typical examples the stability curves of RNase A in the presence of  $\text{NaCl}$ ,  $\text{CsCl}$ , and  $[\text{Me}_4\text{N}]\text{Cl}$ , Fig. 9 illustrates how temperature influences the order of the Hofmeister series. Depending on the temperature (see the vertical lines at 285 K, 315 K, 342 K) different rankings of the cations  $\text{Na}^+$ ,  $\text{Cs}^+$ , and  $[\text{Me}_4\text{N}]^+$  are obtained. While  $[\text{Me}_4\text{N}]^+$  is the least stabilizing cation at high temperatures, it is the most stabilizing cation at low temperatures. The order of  $\text{Na}^+$  and  $\text{Cs}^+$ , which remains the same in the temperature range shown in Fig. 9, changes at high temperatures (around 395 K) as well. Similar temperature depending Hofmeister effects are obtained for the ionic liquids (Fig. 6b).

Ranking ions in a Hofmeister series therefore implies that the underlying cosolute-mechanisms reflect homologous effects. However, the salt-induced changes of the stability curves (Fig. 6–9) and of  $\Delta\Delta H_u$  and  $T\Delta\Delta S_u$  (Fig. 4 and 5) show that this is not the case. Different kind of ions can induce qualitatively different shifts of the  $\Delta G_u(T)$ -curve, which – depending on the temperature – alter the sequence of salts in the Hofmeister series. These crossovers become more important the less the ions have in common (at least in the structural sense). Examples are  $[\text{gdm}]^+$  or  $[\text{Me}_4\text{N}]^+$  within a cation series and complex molecular anions such as  $[\text{SCN}]^-$  or  $[\text{ClO}_4]^-$  within the anion series. However, as discussed in the previous section, even a homologous series such as  $\text{Li}^+$ ,  $\text{Na}^+$ ,  $\text{K}^+$ , and  $\text{Cs}^+$  has outliers ( $\text{Li}^+$ ) when the salt effect is dissected into its thermodynamic mechanisms. The temperature dependence of the Hofmeister series, so far not appreciated in the literature, may explain most outliers in the discussed literature. For example, the non-homologous effects of salt–protein interactions cause a loss of the Hofmeister series upon dissection of the redox potential of cytochrome *c* into the enthalpic and entropic contributions.<sup>62</sup> We suggest that this is due to heterogeneous molecular mechanisms causing the intersections of the respective temperature dependent redox potentials.<sup>62</sup>

## Towards a molecular mechanism

Strictly speaking, thermodynamics cannot provide a molecular mechanism of a reaction. However, comparisons of the thermodynamics of cosolute effects to well characterized cosolutes such as  $[\text{gdm}]\text{Cl}$  or urea could give microscopic insights, although one has to be careful:  $\Delta\Delta H_u$  and  $\Delta\Delta S_u$  include protein as well as solvent terms. Even though the enthalpic and entropic contributions of the solvent terms exactly cancel each other,<sup>63,64</sup> they can be large in comparison to the protein terms and therefore significantly influence the temperature dependence of  $\Delta G_u$ .<sup>65</sup> Thus, similar excess thermodynamic functions



or similar shifts of the stability curve can have different molecular origins.<sup>5</sup>

Today, it is widely accepted that the commonly used protein denaturants urea and [gdm]Cl denature proteins *via* direct chemical interactions.<sup>11,12</sup> The thermodynamic fingerprint of all proteins in the presence of these chemical denaturants is a negative  $\Delta\Delta H_u$  and  $T\Delta\Delta S_u$ .<sup>7,10,30</sup> Based on the thermodynamic fingerprint, the destabilizing Hofmeister effect of NaBr and LiCl (Fig. 5, 7 and 8) could also be founded in chemical interactions of the ions with the protein.

In contrast, the ionic liquids are mainly located in field I of Fig. 5 indicating a different molecular mechanism compared to a typical protein denaturant. This is in accordance with the measurement of transfer free energies of amino acids showing that imidazolium-based ionic liquids interact unfavorably with the protein backbone similar to excluded cosolutes such as polyols and sugars, even so the interaction with the side chains of amino acids is favorable.<sup>66</sup> The increasing trend of  $\Delta\Delta H_u$  and  $T\Delta\Delta S_u$  with increasing hydrophobicity of the cation indicates a molecular mechanism which is directly related to the cosolute effect of alcohols on protein stability.

With increasing the hydrophobicity of the cosolutes, the destabilizing entropic contribution and the counteracting stabilizing enthalpic contribution increase. The effect of a

hydrophobic cosolute on protein thermodynamics is thereby similar to the transfer thermodynamics of a hydrophobic cosolute into water in the observed temperature range.<sup>65</sup> A decrease of entropy is a hallmark of the transfer of a hydrophobic cosolute from the gaseous state into water at temperatures below 100 °C. A reduced entropy of water in an aqueous solution of a hydrophobic cosolute could therefore diminish the reduction of the entropy of water upon unfolding of the protein due to the solvation of exposed hydrophobic residues, since the entropy of water is already reduced due to the presence of the hydrophobic cosolute (Fig. 10). This effect is consistent with a  $\Delta\Delta S_u > 0$  and  $\Delta\Delta H_u > 0$  as experimentally observed by us. A direct binding mechanism (as in the case of [gdm]Cl or urea) which could also explain the reduction of  $T_m$  in ethanol solutions is not likely because the direct interactions between protein and denaturant cause a downshift of the stability curve resulting in  $\Delta G_{u,max,cosolute} < \Delta G_{u,max,buffer}$ . In fact, the stability curve of RNase A in the presence of ethanol resembles a horizontally shifted stability curve of an excluded cosolute instead (Fig. 6a).

## Conclusion

Here we present a novel thermodynamic analysis of cosolute effects on protein stability based on their different impact on the protein stability curve,  $\Delta G_u(T)$ . As the shape of the curve remains the same for different cosolutes, we discussed the effects in terms of shifts of the maximum differently based on their respective enthalpic ( $\Delta\Delta H_u$ ) and entropic ( $T\Delta\Delta S_u$ ) contributions to the excess free energy ( $\Delta\Delta G_u$ ): the more hydrophobic the cosolute, the larger the destabilizing entropic and the stabilizing enthalpic contributions. This classification is valid for both, neutral cosolutes as well as ions and leads to a new understanding of the Hofmeister series. Multiple intersections of the respective  $\Delta G_u(T)$  curves, determined by their thermodynamic fingerprints, manifest themselves in temperature dependent ion rankings. The present thermodynamic analysis is a fundamental framework for future molecular studies and simulations of cosolute effects.

## Acknowledgements

We thank Liel Sapir for helpful discussions. We acknowledge funding from the Cluster of Excellence RESOLV (EXC 1069) funded by the German Research Foundation (DFG). M. S. acknowledges financial support by the Fonds der Chemischen Industrie.

## References

- 1 K. A. Dill, *Biochemistry*, 1990, **29**, 7133–7155.
- 2 R. Lumry and S. Rajender, *Biopolymers*, 1970, **9**, 1125–1227.
- 3 S. B. Zimmerman and S. O. Trach, *J. Mol. Biol.*, 1991, **222**, 599–620.

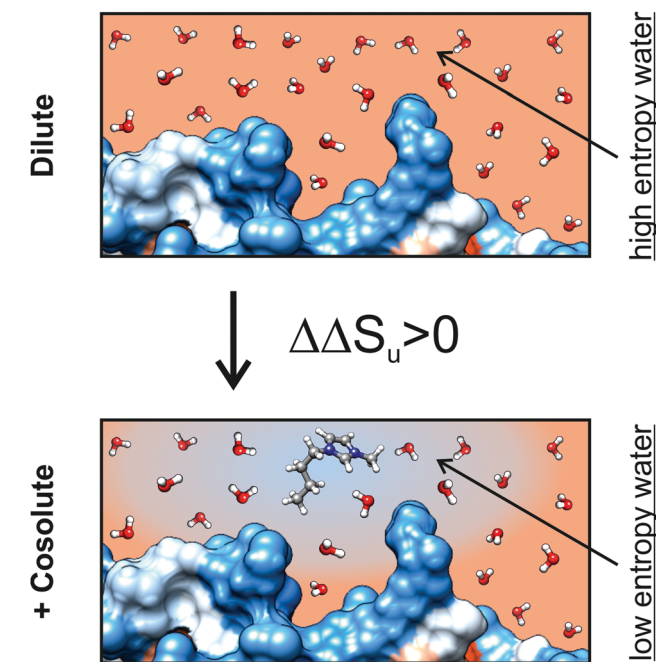


**Fig. 10** Schematic representation of the hydrophobicity surface (blue: hydrophobic, red: hydrophilic) of a protein in dilute solution and in the presence of solvated [bmim]<sup>+</sup>. The scheme illustrates a possible molecular mechanism of a hydrophobic cosolute. The gradient of the background color from blue to red indicates the reduction of water entropy due to the hydration of the hydrophobic groups of [bmim]<sup>+</sup>. The reduced entropy diminishes the loss of entropy due to solvation of hydrophobic groups of the protein which get solvent exposed upon unfolding. This diminished loss of water entropy upon unfolding causes the experimentally observed  $\Delta\Delta S_u > 0$ .



- 4 H. X. Zhou, G. Rivas and A. P. Minton, *Annu. Rev. Biophys.*, 2008, **37**, 375–397.
- 5 L. Sapir and D. Harries, *J. Chem. Theory Comput.*, 2015, **11**, 3478–3490.
- 6 L. A. Benton, A. E. Smith, G. B. Young and G. J. Pielak, *Biochemistry*, 2012, **51**, 9773–9775.
- 7 M. Senske, L. Törk, B. Born, M. Havenith, C. Herrmann and S. Ebbinghaus, *J. Am. Chem. Soc.*, 2014, **136**, 9036–9041.
- 8 P. H. Yancey, M. E. Clark, S. C. Hand, R. D. Bowlus and G. N. Somero, *Science*, 1982, **217**, 1214–1222.
- 9 R. Gilman-Politi and D. Harries, *J. Chem. Theory Comput.*, 2011, **7**, 3816–3828.
- 10 G. I. Makhatadze and P. L. Privalov, *J. Mol. Biol.*, 1992, **226**, 491–505.
- 11 D. R. Canchi and A. E. Garcia, *Annu. Rev. Phys. Chem.*, 2013, **64**, 273–293.
- 12 B. Moeser and D. Horinek, *J. Phys. Chem. B*, 2014, **118**, 107–114.
- 13 F. Hofmeister, *Arch. Exp. Pathol. Pharmacol.*, 1888, **24**, 247–260.
- 14 K. D. Collins and M. W. Washabaugh, *Q. Rev. Biophys.*, 1985, **18**, 323–422.
- 15 W. Kunz, *Curr. Opin. Colloid Interface Sci.*, 2010, **15**, 34–39.
- 16 P. Lo Nostro and B. W. Ninham, *Chem. Rev.*, 2012, **112**, 2286–2322.
- 17 P. Jungwirth and P. S. Cremer, *Nat. Chem.*, 2014, **6**, 261–263.
- 18 P. Ball and J. E. Hallsworth, *Phys. Chem. Chem. Phys.*, 2015, **17**, 8297–8305.
- 19 A. P. dos Santos, A. Diehl and Y. Levin, *Langmuir*, 2010, **26**, 10778–10783.
- 20 Y. Marcus, *Curr. Opin. Colloid Interface Sci.*, 2016, **23**, 94–99.
- 21 R. J. Carlton, C. D. Ma, J. K. Gupta and N. L. Abbott, *Langmuir*, 2012, **28**, 12796–12805.
- 22 M. M. Ries-Kautt and A. F. Ducruix, *J. Biol. Chem.*, 1989, **264**, 745–748.
- 23 Y. Zhang and P. S. Cremer, *Proc. Natl. Acad. Sci. U. S. A.*, 2009, **106**, 15249–15253.
- 24 A. Salis, D. Bilaničová, B. W. Ninham and M. Monduzzi, *J. Phys. Chem. B*, 2007, **111**, 1149–1156.
- 25 D. Bilaničová, A. Salis, B. W. Ninham and M. Monduzzi, *J. Phys. Chem. B*, 2008, **112**, 12066–12072.
- 26 P. H. Von Hippel and T. Schleich, *Acc. Chem. Res.*, 1969, **2**, 257–265.
- 27 J. W. Bye and R. J. Falconer, *Protein Sci.*, 2013, **22**, 1563–1570.
- 28 M. Boström, F. W. Tavares, S. Finet, F. Skouri-Panet, A. Tardieu and B. W. Ninham, *Biophys. Chem.*, 2005, **117**, 217–224.
- 29 L. M. Pegram, T. Wendorff, R. Erdmann, I. Shkel, D. Bellissimo, D. J. Felitsky and M. T. Record, Jr., *Proc. Natl. Acad. Sci. U. S. A.*, 2010, **107**, 7716–7721.
- 30 S. Sukenik, L. Sapir, R. Gilman-Politi and D. Harries, *Faraday Discuss.*, 2013, **160**, 225–237, discussion 311–227.
- 31 M. Yamasaki, H. Yano and K. Aoki, *Int. J. Biol. Macromol.*, 1991, **13**, 322–328.
- 32 D. F. Parsons and A. Salis, *Curr. Opin. Colloid Interface Sci.*, 2016, **23**, 41–49.
- 33 W. J. Becktel and J. A. Schellman, *Biopolymers*, 1987, **26**, 1859–1877.
- 34 H. Weingärtner, *Angew. Chem., Int. Ed.*, 2008, **47**, 654–670.
- 35 H. Weingärtner, C. Cabrele and C. Herrmann, *Phys. Chem. Chem. Phys.*, 2012, **14**, 415–426.
- 36 F. van Rantwijk and R. A. Sheldon, *Chem. Rev.*, 2007, **107**, 2757–2785.
- 37 D. Constantinescu, H. Weingärtner and C. Herrmann, *Angew. Chem., Int. Ed.*, 2007, **46**, 8887–8889.
- 38 M. Senske, S. Ebbinghaus and C. Herrmann, in *Foundations and Contemporary Approaches*, ed. M. Bastos, 2016, ch. 13, pp. 247–259.
- 39 D. Constantinescu, C. Herrmann and H. Weingärtner, *Phys. Chem. Chem. Phys.*, 2010, **12**, 1756–1763.
- 40 P. L. Privalov and G. I. Makhatadze, *J. Mol. Biol.*, 1990, **213**, 385–391.
- 41 R. Ravindra and R. Winter, *Z. Phys. Chem.*, 2003, **217**, 1221–1243.
- 42 P. L. Privalov, *Crit. Rev. Biochem. Mol. Biol.*, 1990, **25**, 281–305.
- 43 G. I. Makhatadze, M. M. Lopez, J. M. Richardson, 3rd and S. T. Thomas, *Protein Sci.*, 1998, **7**, 689–697.
- 44 C. Q. Hu, J. M. Sturtevant, J. A. Thomson, R. E. Erickson and C. N. Pace, *Biochemistry*, 1992, **31**, 4876–4882.
- 45 C. N. Pace and G. R. Grimsley, *Biochemistry*, 1988, **27**, 3242–3246.
- 46 C. Lange, G. Patil and R. Rudolph, *Protein Sci.*, 2005, **14**, 2693–2701.
- 47 Y. Shu, M. Liu, S. Chen, X. Chen and J. Wang, *J. Phys. Chem. B*, 2011, **115**, 12306–12314.
- 48 A. M. Figueiredo, J. Sardinha, G. R. Moore and E. J. Cabrita, *Phys. Chem. Chem. Phys.*, 2013, **15**, 19632–19643.
- 49 P. Attri, P. Venkatesu and A. Kumar, *Phys. Chem. Chem. Phys.*, 2011, **13**, 2788–2796.
- 50 N. K. Poddar, Z. A. Ansari, R. K. B. Singh, A. A. Moosavi-Movahedi and F. Ahmad, *Biophys. Chem.*, 2008, **138**, 120–129.
- 51 Y. F. Liu and J. M. Sturtevant, *Biochemistry*, 1996, **35**, 3059–3062.
- 52 S. S. Cho, G. Reddy, J. E. Straub and D. Thirumalai, *J. Phys. Chem. B*, 2011, **115**, 13401–13407.
- 53 J. F. Brandts and L. Hunt, *J. Am. Chem. Soc.*, 1967, **89**, 4826–4838.
- 54 G. Velicelebi and J. M. Sturtevant, *Biochemistry*, 1979, **18**, 1180–1186.
- 55 S. R. Martin, V. Esposito, P. De Los Rios, A. Pastore and P. A. Temussi, *J. Am. Chem. Soc.*, 2008, **130**, 9963–9970.
- 56 O. Miyawaki and M. Tatsuno, *J. Biosci. Bioeng.*, 2011, **111**, 198–203.
- 57 A. E. Smith, L. Z. Zhou, A. H. Gorensek, M. Senske and G. J. Pielak, *Proc. Natl. Acad. Sci. U. S. A.*, 2016, **113**, 1725–1730.
- 58 M. Senske, A. E. Smith and G. J. Pielak, *Angew. Chem., Int. Ed.*, 2016, **55**, 3586–3589.
- 59 N. Schwierz, D. Horinek, U. Sivan and R. R. Netz, *Curr. Opin. Colloid Interface Sci.*, 2016, **23**, 10–18.



- 60 S. C. Flores, J. Kherb, N. Konelick, X. Chen and P. S. Cremer, *J. Phys. Chem. C*, 2012, **116**, 5730–5734.
- 61 N. Schwierz, D. Horinek and R. R. Netz, *Langmuir*, 2013, **29**, 2602–2614.
- 62 L. Medda, A. Salis and E. Magner, *Phys. Chem. Chem. Phys.*, 2012, **14**, 2875–2883.
- 63 A. Ben-Naim, *Biopolymers*, 1975, **14**, 1337–1355.
- 64 H.-A. Yu and M. Karplus, *J. Chem. Phys.*, 1988, **89**, 2366–2379.
- 65 D. Ben-Amotz, *Annu. Rev. Phys. Chem.*, 2016, **67**, 617–638.
- 66 A. Tischer, H. Lilie, M. Auton and C. Lange, *Biopolymers*, 2014, **101**, 1129–1140.

